An optical leaky wave antenna with silicon perturbations for electronic control

Salvatore Campione, Qi Song, Ozdal Boyraz[#], Filippo Capolino*
Dept. of Electrical Engineering and Computer Science, University of California, Irvine, CA 92697-2625, USA

ABSTRACT

An optical leaky wave antenna (OLWA) is a device that radiates a light wave into the surrounding space from a leaky wave (LW) guided mode or receives optical power from the surrounding space into a guided optical mode. In this work, we propose and provide a 3D analysis of a novel CMOS compatible OLWA made of a silicon nitride (Si_3N_4) waveguide comprising periodic silicon perturbations which allow electronic tuning capability. The analysis presented here includes the effect of the number of semiconductor perturbations, the antenna radiation pattern and directivity. We show that the number of the silicon perturbations has to be large to provide a long radiating section required to achieve radiation with high directivity. In other words, the proposed structure allows for a very narrow-beam radiation. Preliminary results are confirmed by exploiting leaky wave and antenna array factor theory, as well as verified by means of two full-wave simulators (HFSS and COMSOL). Our purpose is to ultimately use PIN junctions as building blocks for each silicon implantation for the electronic control of the radiation. In particular, the electronic tunability of the optical parameters of silicon (such as refractive index and absorption coefficient) via current injection renders itself the ideal platform for optical antennas that can facilitate electronic beam control, and boost the efficiency of optoelectronic devices such as light-emitting diodes, lasers and solar cells, and bio-chemical sensors.

Keywords: optical leaky wave antenna (OLWA), CMOS compatible, subwavelength structures, waveguides, silicon on insulator (SOI), electronic tunability.

1. INTRODUCTION AND STATEMENT OF THE PROBLEM

An optical leaky wave antenna (OLWA) is a device that radiates a light wave into the surrounding space from a leaky wave (LW) guided mode or, vice-versa, it couples receiving optical power from the surrounding space into a guided optical mode. Optical antennas have the capabilities to enhance the interaction between light and matter, and thus have the potential to boost the efficiency of optoelectronic devices such as light-emitting diodes, lasers and solar cells, and bio-chemical sensors [1-3].

In [4], we have proposed the design of a dielectric (silicon nitride) OLWA with periodic semiconductor (silicon) perturbations, capable of producing narrow beam radiation, with electronic tuning capability. The optical antenna cases studied up to date mostly focus on the local field distribution control of the device. Those kinds of antennas are fabricated in a sub-wavelength dimension and some exceptional physical phenomena, such as super-resolution effect and near-field enhancement [5], are realizable due to the resonant modes. In the optoelectronics domain, silicon-on-insulator (SOI) devices have been widely utilized recently to deliver chip scale active and passive photonic devices such as amplifiers, switches and modulators with potential optoelectronic integration on the same platform [6-7]. The silicon on insulator (SOI) based planar waveguide provides tight mode confinement due to a large index contrast, which is essential for miniaturization, and simultaneous low loss operation [8]. In particular, the use of silicon offers the electronic tunability for optical parameters of silicon (such as refractive index and absorption coefficient) via current injection. Combination of optical antennas with silicon perturbation can facilitate electronic beam control for OLWAs [9-11]. Hence, the OLWA can function as a passive transmitter or receiver as well as beam steering device [4].

oboyraz@uci.edu; phone 1 949-824-1979; http://apdsl.eng.uci.edu/

* f.capolino@uci.edu; phone 1 949-824-2164; http://capolino.eng.uci.edu/

Photonic Fiber and Crystal Devices: Advances in Materials and Innovations in Device Applications V, edited by Shizhuo Yin, Ruyan Guo, Proc. of SPIE Vol. 8120, 81200G · © 2011 SPIE · CCC code: 0277-786X/11/$18 · doi: 10.1117/12.896227

The OLWA proposed here radiates a narrow beam because a leaky wave (LW) with low attenuation constant is excited at one end of the dielectric waveguide with perturbations. Accordingly, the periodicity of the silicon perturbations of the waveguide produces a spatial harmonic of the guided mode in the visible region. Here we show that pointing angle, beam-width, and operational frequency are all related to the LW complex wavenumber, whose value depends on the amount of silicon perturbations in the waveguide [4]. Also, the propagation constant and the attenuation coefficient of the LW in the periodic structure are extracted from full-wave simulations. The number of silicon perturbations and their effect on the radiation pattern is investigated to obtain a directive compact emitter.

The structure of the paper is as follows. The structure of the proposed OLWA is presented in Sec. 2. Then, the two theoretical models used to predict the radiation pattern of the OLWA are summarized in Sec. 3. In Sec. 4 we describe the performance of the OLWA, and we observe the radiation pattern tunability due to the usage of electronic control of PIN junctions in Sec. 5.

2. PROPOSED STRUCTURE AND FULL-WAVE SIMULATION RESULTS

The first difficulty in the 3D implementation arises from the design of a single mode rectangular dielectric waveguide (it is well known that the fundamental mode cannot be avoided in this kind of waveguides); we adopt approximate formulation for optical fibers on the normalized frequency V to have a starting point for the design of the wave guiding structure. Also, the waveguide cross section cannot be too small otherwise it cannot confine most of the energy injected into the structure in the core. Taking care of all the previous conditions, the proposed structure is reported in Fig. 1. The waveguide is made of silicon nitride (Si_3N_4) with refractive index equal to 1.67, is positioned along the x direction and is $49.285\ \mu m$ long; it has a square cross section of $w \times w$, with $w = 1\ \mu m$ in the yz plane.

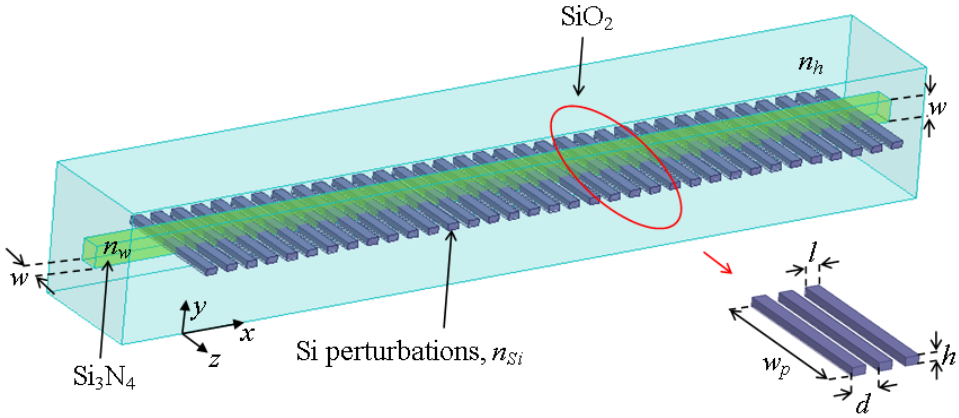

Fig. 1. The 3D structure of the proposed OLWA made of silicon nitride (Si_3N_4) in glass, with dimensions, with silicon perturbations extended to the edge of the glass background. The OLWA is fed by a mode in the silicon nitride waveguide from the left. The edges of Si strips can be connected to electrodes for injecting carriers in the intrinsic Si region.

The silica glass computational domain has a refractive index equal to 1.45, is $49.285\ \mu m$ long along the x direction and $6\ \mu m$ in both the y and z directions. To provide direct radiation, we choose to utilize $N = 35$ elements, made of silicon, with refractive index equal to 3.48, positioned periodically along the x direction $14.03175\ \mu m$ away from the antenna's input side (on the left in Fig. 1). The perturbation is periodic along x with period d (each element has a length equal to $d/2$), has a height of $h = 0.3\ \mu m$ along y and has a width equal to $w_p = 6\ \mu m$ in the z direction. A guided wave is injected from the left side of the antenna, polarized along z. When this guided wave encounters the periodic silicon perturbations, it transitions into a leaky wave (LW), with radiating Floquet harmonic characterized by $k_{-1} = \beta_{-1} + i\alpha$, with $\beta_{-1} = k_0 n_{eff} - 2\pi / d$, $k_0 = 2\pi / \lambda_0$, slowly decaying while traveling along the waveguide. The period d of the perturbation is then designed to provide radiation at broadside in the xy plane (i.e., along y). Indeed, this happens when $\cos\phi = \beta_{-1} / k_0 \approx 0$, or when $\beta_{-1} = k_0 n_{eff} - 2\pi / d = 2\pi\left(1/\lambda_{eff} - 1/d\right) \approx 0$, which implies $d \approx \lambda_{eff} = 1.015\ \mu m$. The length of the perturbations is then $L = Nd$. The working free space wavelength is $\lambda_0 = 1.55\ \mu m$.

3. THEORETICAL MODELS

Here we adapt two theoretical models (equivalent aperture model and array factor model) to predict the radiation pattern of the OLWA and to provide guidance for further design modifications.

3.1 Floquet theory

As previously mentioned in Sec. 2, the guided mode excited by the incoming field on the left side of the waveguide becomes leaky in correspondence of the periodic silicon perturbations. Such a mode decays exponentially along the structure, even for a lossless structure, and a leakage phenomenon (radiation) takes place.

The electric field is polarized along z and travels along the x direction. The z-component of the guided electric field satisfies the quasi-periodic property $E(x+d,y)=E(x,y)\exp(ik_{x,0}d)$, where d is the period of the periodic structure and $k_{x,0}=\beta+i\alpha$ is the wavenumber along the propagation direction. Here, β and α are the phase and attenuation constants, respectively, of the LW. Note that, before introducing the perturbations, the original guided mode has a phase propagation constant very close to β, whereas the attenuation constant of the waveguide would be much smaller than α (without perturbation the attenuation is caused only by material losses and scattering by irregularities of the structure). Instead, with perturbations, the value of α can be significantly large because of radiation, though to have a directive OLWA this value has to be maintained low. Accordingly, in terms of a Fourier series expansion, the electric field at any place along the periodic structure can be represented as the superposition of Floquet spatial harmonics

$$E(x,y)=\sum_{n=-\infty}^{\infty}E_n(y)e^{ik_{x,n}x},\quad k_{x,n}=k_{x,0}+2n\pi/d, \tag{1}$$

where $k_{x,n}$ is the Floquet wavenumber, n is the order of the Floquet spatial harmonic, and $E_n(y)$ is the weight of the n-th harmonic [12-14]. Each Floquet wave number $k_{x,n}=\beta_n+i\alpha$ has the same attenuation constant α. The purpose of the periodic perturbations is to create a radiating $n=-1$ harmonic. Its wavenumber is

$$k_{x,-1}=\beta_{-1}+i\alpha,\ \text{with}\ \beta_{-1}=\beta-2\pi/d, \tag{2}$$

such that $-k_h<\beta_{-1}<k_h$, where $k_h=n_hk_0$, k_0 is the free space wavenumber, and n_h is the refractive index of the surrounding material, that in our case is free space ($n_h=1$).

Therefore, in the periodic structure under analysis, all the n-indexed Floquet harmonics but one are evanescent waves (contrarily to what may happen in gratings where several harmonics have β_n in the visible region, i.e., the wavenumber region $-k_h<\beta_n<k_h$ relative to waves that can propagate away from the plane). The radiating harmonic, the one that falls in the interval $(-k_h,k_h)$, is usually defined as the $n=-1$ one since in slightly perturbed structures the 0^{th} fundamental propagation constant $\beta\equiv\beta_0>k_h$ has a value very close to the one of the bound mode in the unperturbed waveguide, and thus it is not radiating.

3.2 Equivalent aperture (EA) model

Based on the Floquet field expansion (1), the electric field along the periodic structure can be described as a superposition of field terms, and only the $n=-1$ is relevant for radiation. Therefore, its expression evaluated on the "aperture" (i.e, a section from where we assume radiation is propagating away [15]) is

$$E(x)=E_{-1}e^{i\beta_{-1}x}e^{-\alpha x}\qquad(0<x<L), \tag{3}$$

where L is the total length of the silicon perturbation, and E_{-1} is the amplitude of the $n=-1$ harmonic of the electric field at the beginning of the silicon perturbation.

The beam radiation angle is related to the $n=-1$ spatial harmonic propagation constant in (2) by the expression $\beta_{-1}=k_h\cos\phi$; therefore, radiation at broadside (i.e., direction orthogonal to the waveguide, at angle $\phi=\pm\pi/2$) is then obtained when $\beta_{-1}<<k_h$.

The far-field radiation pattern $E^{FF}(\phi)$ is obtained by integrating (3) across an "equivalent aperture" $(0<x<L)$ which leads to a normalized far-field pattern magnitude

$$F(\phi)=\left(\frac{1+e^{-2\alpha L}-2e^{-\alpha L}\cos\left[\left(k_h\cos\phi-\beta_{-1}\right)L\right]}{\left(k_h\cos\phi-\beta_{-1}\right)^2+\alpha^2}\right)^{\frac{1}{2}}, \tag{4}$$

that in the case of large αL (either when the antenna is long, or when the attenuation constant is large) can be further simplified.

3.3 Array factor (AF) model

In the array factor method instead, the periodic perturbation can be considered as an array of identical scatterers. The far-field pattern is then obtained by multiplying the pattern of the single element (quasi isotropic) and the array factor (AF) of the array (very angle-selective) [16]. As usual for directive antennas the total far field radiation pattern is approximated as $E^{FF}(\phi)\propto AF(\phi)$. For the OLWA under consideration, the magnitude of the array factor $AF(\phi)$ is defined as

$$\left|AF(\phi)\right|=\left(\frac{1+e^{-2\alpha L}-2e^{-\alpha L}\cos\left[\left(k_h\cos\phi-\beta_{-1}\right)L\right]}{1+e^{-2\alpha d}-2e^{-\alpha d}\cos\left[\left(k_h\cos\phi-\beta_{-1}\right)d\right]}\right)^{\frac{1}{2}}, \tag{5}$$

where we have assumed that $L=Nd$. An analogous procedure was applied in [17] to find the directive radiation pattern of a narrow slit in a corrugated silver film.

4. ANTENNA RADIATION CAPABILITIES

The accuracy of theoretical models is compared with full-wave numerical simulations. In particular we use 3D modeling by using HFSS and COMSOL as described below.

4.1 Guiding properties and scattering parameters

The maps of the electric field magnitude at the input side and along a *xy* plane section in the center of the waveguide are shown in Fig. 2; the former shows good power confinement within the core, whereas the latter shows that the leaky wave slowly decays along the silicon perturbations. We also computed the scattering parameters of the antenna, considering two waveports ($4\ \mu\text{m}\times 4\ \mu\text{m}$) located at the beginning and at the end of the waveguide. The reflection coefficient $S_{11}=-15$ dB shows that a negligible amount of the power injected into the antenna is reflected back. The transmission coefficient $S_{12}=-21$ dB shows that a radiation phenomenon is taking place, since the dielectric materials are considered to have negligible losses. In case power is still present at the end of the waveguide, a higher number of silicon perturbations could be required to radiate all the power injected into the antenna.

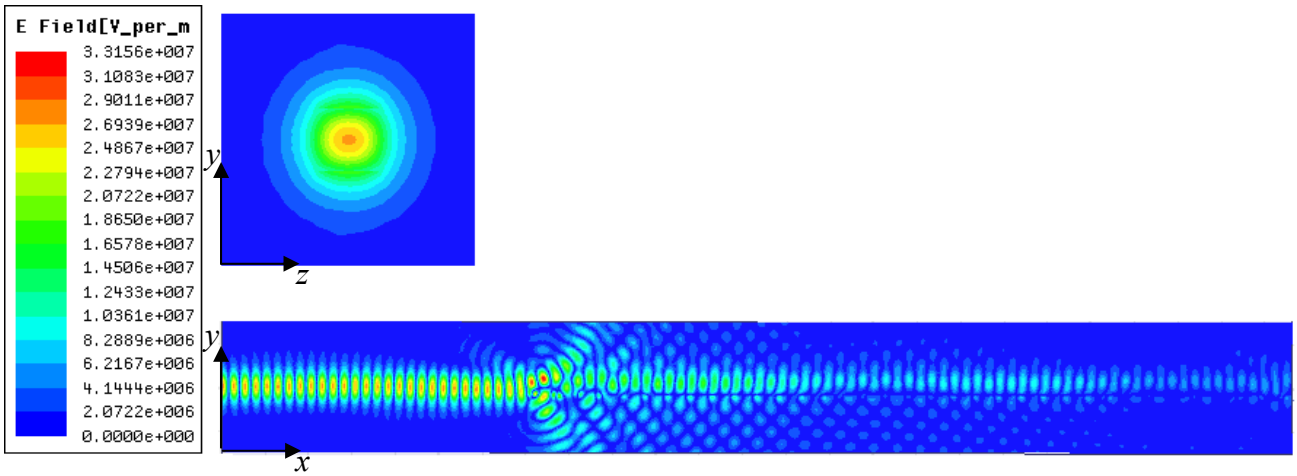

Fig. 2. Map of the magnitude of the electric field ($|\mathbf{E}(\mathbf{r},t)|$) at the input side (transverse square cross section with size $4\ \mu\text{m} \times 4\ \mu\text{m}$, and along a longitudinal (*x*-*y* plane) section at the center of the waveguide (result from HFSS simulation). One may notice the field scattered at the beginning of the perturbation section, and leakage from the perturbed waveguide.

4.2 Extraction of the leaky wave parameters

As stated in Sec. 3.1, the excited leaky mode decays exponentially along the structure, even for a lossless structure, and a leakage phenomenon (radiation) takes place.

To better extract the leaky wave theory parameters β_{-1} and α we simulate a 70 elements long perturbation by resorting to PEC/PMC symmetry planes at the right end side of the waveguide. Indeed, we know that the local field magnitude decays exponentially along the perturbed waveguide with attenuation constant α. Moreover, its phase shift is linearly dependent to the propagation constant, as can be seen looking at the phase term $\beta_{-1}x$.

Figure 3(a) and 3(b) show the field magnitude and phase (obtained from HFSS) along the silicon-perturbed waveguide, sampled at one point per cell, positioned at the center of each Si perturbation, along *x,* for two different positions along *y*: (i) at the bottom of each Si perturbation, and (ii) in the middle of the waveguide. The magnitude of the field $E(x)$ in Fig. 3(a) exhibits a linear trend using a logarithmic scale, confirming its exponential decay along the waveguide longitudinal direction as expected from $|E(x)/E_{-1}|_{\text{dB}} = 20\log e^{-\alpha x} = -20\alpha x \log e$. As can be easily inferred, the attenuation constant α can be measured from the slope of the line in Fig. 3(a). Figure 3(b) shows, instead, the unwrapped phase $\beta_{-1}x$ of the leaky wave along the waveguide: the slope of the line provides the propagation constant β_{-1}. Observing one sample of the field per period gives us only the phase propagation constant in the main Brillouin zone.

We perform a linear fitting of the extracted data reported in Fig. 3 (more precise estimation would however be based on finding the complex wavenumber in a fully periodic waveguide). The leaky wave theory parameters are $\beta_{-1} = -2.18\times10^{5}\text{m}^{-1}$ ($\beta_{-1}/k_0 \approx -0.05$) and $\alpha = 4.80\times10^{4}\text{m}^{-1}$ ($\alpha/k_0 \approx 0.01$) (middle waveguide) or $\beta_{-1} = -2.19\times10^{5}\text{m}^{-1}$ ($\beta_{-1}/k_0 \approx -0.05$) and $\alpha = 4.82\times10^{4}\text{m}^{-1}$ ($\alpha/k_0 \approx 0.01$) (bottom waveguide) extracted by the decaying field along the perturbations shown in Fig. 3. This result proves that the field decays in the same way in every section of the waveguide.

We then compare in Fig. 4 the decaying field in the bottom side of the waveguide from HFSS with the one obtained by a COMSOL simulation. The leaky wave theory parameters from COMSOL are $\beta_{-1} = -2.25\times10^{5}\text{m}^{-1}$ ($\beta_{-1}/k_0 \approx -0.055$) and $\alpha = 4.67\times10^{4}\text{m}^{-1}$ ($\alpha/k_0 \approx 0.01$) (bottom waveguide) extracted by the decaying field along the perturbations shown in Fig. 4. The two results are in good agreement.

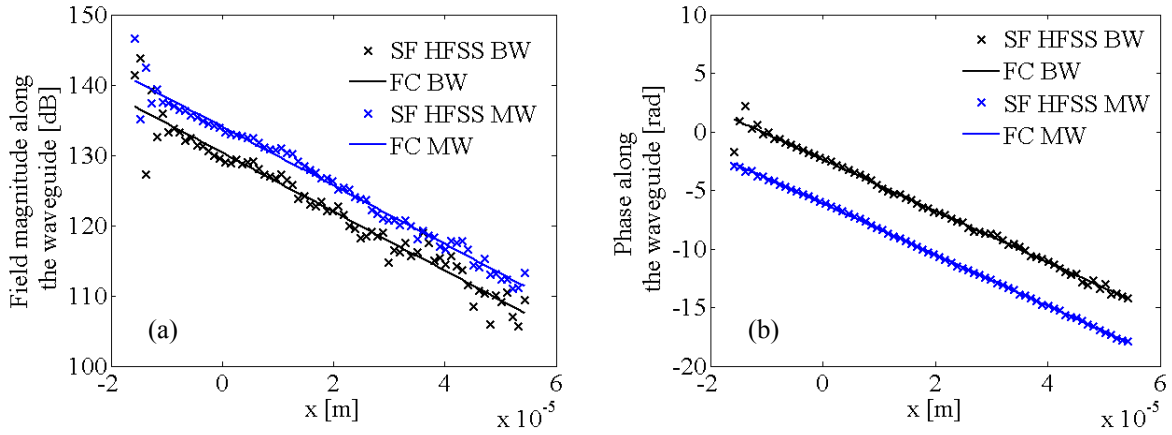

Fig. 3. (a) Field magnitude and (b) phase along the waveguide, sampled one point per silicon element, at the bottom side and in the middle of the waveguide for 70 element silicon perturbations (from HFSS simulation).

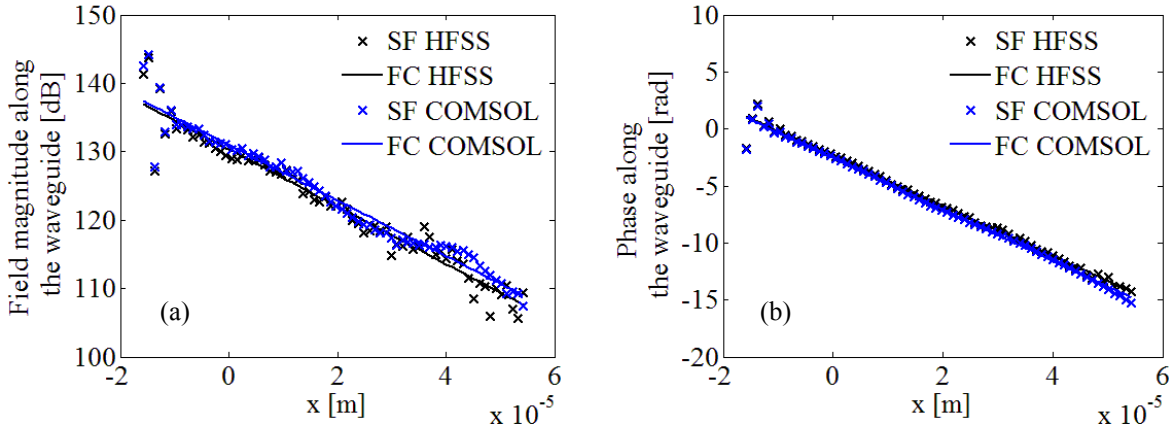

Fig. 4. (a) Field magnitude and (b) phase along the waveguide, sampled one point per silicon element, at the bottom side of the waveguide for a 70 element perturbations (comparison between COMSOL and HFSS simulations).

4.3 Radiation pattern

The radiation patterns from the HFSS and COMSOL simulations from previous section are then compared to the theoretical fields with the extracted parameters from HFSS field decay (bottom waveguide), with leaky wave parameters $\beta_{-1} = -2.19\times10^{5}\,\mathrm{m}^{-1}$ ($\beta_{-1}/k_0 \approx -0.05$) and $\alpha = 4.82\times10^{4}\,\mathrm{m}^{-1}$ ($\alpha/k_0 \approx 0.01$).

A side-lobe is present in the full-wave simulations (not predicted by theory); its presence is due to a certain phase coherence at the beginning of the silicon perturbations. This coherence can be explained by the fact that the first few elements of the perturbation form a subarray that radiates at a certain maximum direction (i.e. the first side-lobe level, around $-53°$) different from the maximum radiation direction of the remaining part of the perturbation (main-lobe, around $-93°$).

To understand how directive the radiation is, we look at the 3 dB beam-width, defined as $\Delta\phi_{3\mathrm{dB}} = \left|\phi^{+}_{3\mathrm{dB}} - \phi^{-}_{3\mathrm{dB}}\right|$, where $F(\phi^{\pm}_{3\mathrm{dB}}) = F(\phi_{\max})/\sqrt{2}$, where F is defined as in (4). By looking at either the simulated HFSS or COMSOL result, $\Delta\phi_{3\mathrm{dB}} \approx 2.5°$.

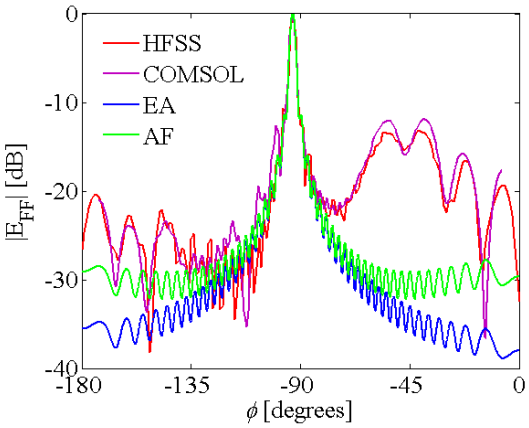

Fig. 5. Comparison of the radiation pattern in the *x-y* plane, obtained by HFSS and COMSOL, and also by the two theoretical models.

4.4 Reducing the number of silicon perturbations to have a compact emitter

We decrease the number of silicon perturbations and we compute and compare the radiation patterns in Fig. 6. It can be observed that the beam widens by decreasing the number of silicon elements (to remark that a long radiating section is needed to obtain high directivity). As such, we computed the 3 dB beam width for the three shown cases, and we got about $\Delta\phi_{3\text{dB}} \approx 2.5°$, $\Delta\phi_{3\text{dB}} \approx 2.9°$ and $\Delta\phi_{3\text{dB}} \approx 3.3°$ for 35, 30 and 25 perturbations, respectively.

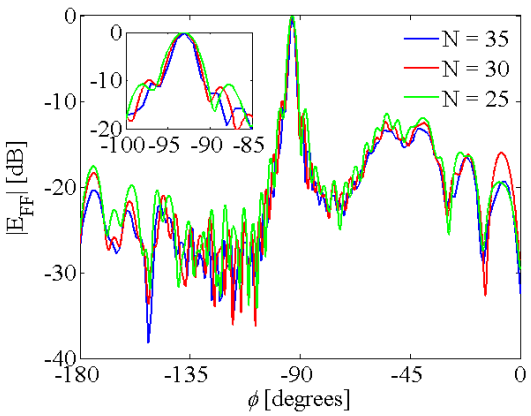

Fig. 6. Radiation pattern in the *x-y* plane for different number of silicon perturbations.

5. ELECTRONIC CONTROL OF THE RADIATION

The use of silicon and SOI technology provides opportunities for opto-electronic integration. As an indirect bandgap material, silicon is highly transparent for optical communication wavelengths. The use of free carrier plasma dispersion effect [18] can induce changes in refractive index and absorption coefficient, which are two critical parameters in OLWA radiation pattern. Up to date plenty of work has been conducted to utilize this nonlinear effect to realize modulation in electro-optic device [7,19]. Here we propose to use silicon perturbations with PIN junction diode structure in OLWAs to control the radiation pattern.

5.1 PIN junction modeling

Figure 7 illustrates the figurative representation of a single silicon perturbation cell with a PIN diode structure. To ensure low loss operation the intrinsic region is placed under the silicon nitride waveguide region. In order to realize the electronic tuning of OLWAs, the carrier density in the intrinsic region is changed by current injection.

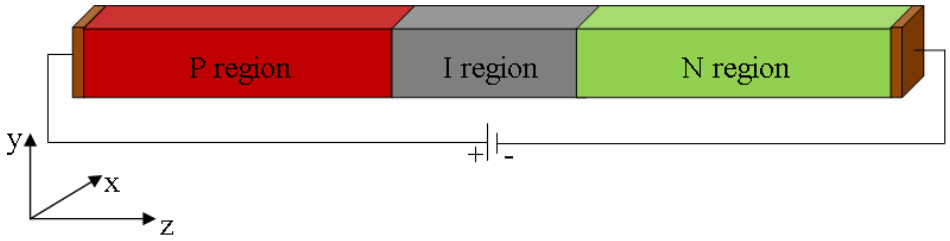

Fig. 7. PIN junction as silicon perturbation unit of OLWA and carrier injection medium. The silicon intrinsic region is at the bottom of the silicon nitride waveguide. The P and N region are not simulated into the EM simulations.

To estimate the electronic response of the OLWA we use a PIN diode structure with $0.5075\ \mu m \times 0.3\ \mu m \times 6\ \mu m$ dimensions, and the P and N regions extends from each side of I region (N_A and N_D are the doping concentrations of P and N region, respectively). The device is simulated by using a two-dimensional (in the y-z plane) simulation module in COMSOL multiphysics. In the model, Shockley-Read-Hall recombination effect is included and the trapped level lifetimes of electrons and holes are considered to be $\tau_e' = \tau_h' = 0.1\ \mu s$. The ohmic contact is assumed at anode and cathode sides. The doping profile of each region is defined as an abrupt step junction for simplicity. The concentration dependent mobility of electrons and holes is calculated based on empirical equations given in [20]. The current and the ambipolar lifetime of the PIN diode are calculated to derive more accurate carrier distribution in the intrinsic region, furthermore, to achieve better estimation of the possible refractive index change and attenuation. The relationship of PIN current with respect to bias voltage is plotted in Fig. 8 for $N_A = N_D = 10^{18}\ \text{cm}^{-3}$ and $N_A = N_D = 10^{19}\ \text{cm}^{-3}$, respectively for forward bias voltages varying from 0 to 5V.

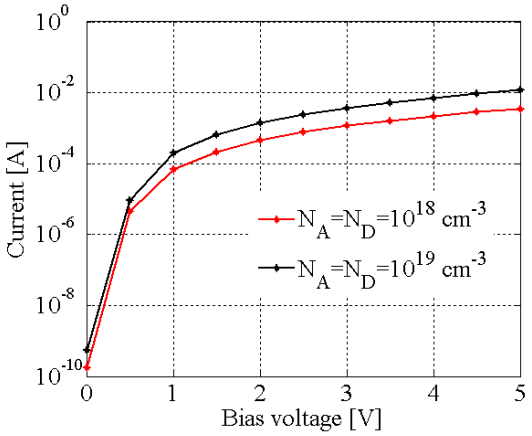

Fig. 8. The current with respect to bias voltage.

We then consider the current flow due to electron-hole recombination in I region. The current density (*n* for electrons and *p* for holes) is given by [20]

$$J_{n,p} = \int_0^{w_p} qUdz = \frac{qn'w_p}{\tau_{e,h}} \tag{6}$$

where $U = n'/\tau_{e,h}$ is the net generation-recombination rate, n' is the average injected electron or hole concentrations in the intrinsic region, $\tau_{e,h}$ are the lifetimes of electrons or holes, $q = 1.6 \times 10^{-19}$ C , and w_p is the width of intrinsic region in the z direction (as in Fig. 1). Here we assume that the carrier concentration throughout the intrinsic region is approximately constant and diffusion current can be neglected as well.

The carrier distribution in intrinsic region can be estimated based on equation (7), from simulated current density and lifetime results. In Fig. 9, electrons and holes distribution can both reach 10^{19} cm^{-3} at current of 7×10^{-4} A for $N_A = N_D = 10^{18}$ cm^{-3}, and at current of 3×10^{-5} A for $N_A = N_D = 10^{19}$ cm^{-3}. From PIN device modeling, high carrier distribution up to 10^{20} cm^{-3} can be achievable within 5V bias voltage for $N_A = N_D = 10^{19}$ cm^{-3}. However, in this last case, Auger processes, which is neglected here, should be taken into account for accurate estimation [21].

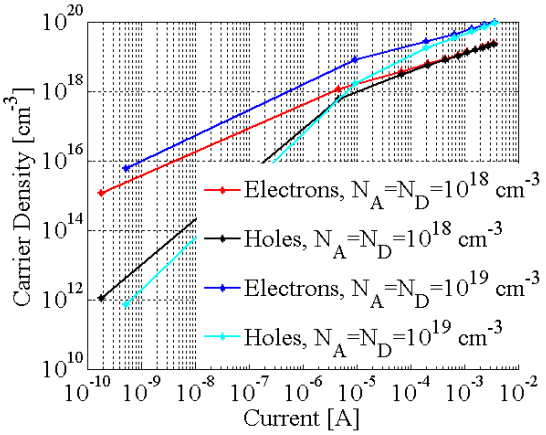

Fig. 9. Carrier density with respect to driving current.

5.2 Electronic control capabilities

From previous analyses, we know that the radiation pattern at the transverse direction highly depends on the attenuation coefficient of the antenna and the effective index. According to Fig. 9, if we set the doping concentration to $N_A = N_D = 10^{18}$ cm^{-3}, and we provide enough bias to obtain around $10^{-5} - 10^{-4}$ A, we obtain carrier density concentrations for both electron and holes to be equal and around $10^{18} - 10^{19}$ cm^{-3}, respectively. This carrier density can alter both the real and imaginary parts of the Si refractive index (unitless) as described by the Drude's model [22]

$$\Delta n_{Si}\left(N_e, N_h\right) = -\left(8.8\times10^{-4} N_e + 8.5 N_h^{0.8}\right)\times10^{-18}, \tag{7}$$

$$\Delta k_{Si}\left(N_e, N_h\right) = \frac{\left(8.5 N_e + 6.0 N_h\right)\times10^{-16}}{k_0}, \tag{8}$$

where N_e and N_h are the concentrations of electrons and holes (expressed in cm^{-3}) in Si, and k_0 is the free space wavenumber (expressed in m^{-1}). In a first order approximation, the modified propagation constant in presence of carrier injection can be expressed as $\beta'_{-1} = \beta_{-1} + ff\,\Delta n_{Si} k_0$, where ff is the filling factor of silicon perturbations (i.e., the percentage of Si volume per unit cell of the OLWA); whereas the attenuation constant in presence of carrier injection can be expressed as $\alpha' = \alpha + ff\,\Delta\bar{\alpha}_{Si} k_0$. According to this model, β'_{-1} should become more negative than β_{-1} (because Δn_{Si} is negative), whereas α' should increase. Using $N_e = N_h = 10^{18}, 10^{19}$ cm^{-3}, we extract again the leaky wave parameters, obtaining $\beta_{-1} = -2.21\times10^5$ m^{-1} ($\beta_{-1}/k_0 \approx -0.054$) and $\alpha = 4.94\times10^4$ m^{-1} ($\alpha/k_0 \approx 0.012$), and $\beta_{-1} = -2.23\times10^5$ m^{-1} ($\beta_{-1}/k_0 \approx -0.055$) and $\alpha = 4.64\times10^4$ m^{-1} ($\alpha/k_0 \approx 0.01$), for $10^{18} - 10^{19}$ cm^{-3}, respectively. The case without carrier injection had the following parameters: $\beta_{-1} = -2.19\times10^5$ m^{-1} ($\beta_{-1}/k_0 \approx -0.05$) and $\alpha = 4.82\times10^4$ m^{-1} ($\alpha/k_0 \approx 0.01$). It can be observed that the values of β_{-1} in absence and in presence of carrier injection follow the approximate model of small perturbations mentioned above. Regarding α however, the linear fitting method is very sensible and does not allow the estimation of small variations: future studies will involve the estimation based on finding the complex wavenumber in a fully periodic waveguide.

Practically, as stated in the previous section, the density of electrons and holes in Si can be increased up to $10^{19}\,\mathrm{cm}^{-3}$ in optoelectronic devices via current injection or photo generation before Auger process starts to mitigate the device performance [23]. Future studies will take this process into account, trying to reach concentrations up to $10^{20}\,\mathrm{cm}^{-3}$ to facilitate more pronounced tunability. Also, future works will involve amplifying weak perturbations in the optical domain by placing perturbations into optical resonators so that these perturbations will be experienced by the optical field during multiple roundtrips [24]. Indeed, it has been already demonstrated theoretically and experimentally that weak perturbations created via injection of carriers into silicon optical resonators alter the resonance wavelength and the quality factor of the resonator and provide modulation of the optical signals [24]. Similarly, by integrating OLWAs into a racetrack or Fabry-Perot integrated cavities, it is expected to amplify the variation in the radiation pattern of an amount which is proportional to the quality factor of the cavity. Future research should be dedicated to quantify the perturbations in the radiation pattern in resonators with practical geometries.

6. CONCLUSION

We have shown the performance of an optical leaky wave antenna (OLWA) able to produce very directive radiation at 193 THz. With a periodic set of PIN junction perturbation little control is exerted on the radiated beam. Enhanced control will be studied in the future by inserting the OLWA into a ring resonator.

ACKNOWLEDGEMENTS

This work is supported by NSF Award # ECCS-1028727. The authors also thank Ansys and COMSOL Multiphysics for providing them their simulation tools (HFSS and COMSOL) that were instrumental in this analysis.

REFERENCES

[1] P. Ghenuche, S. Cherukulappurath, T. H. Taminiau *et al.*, "Spectroscopic mode mapping of resonant plasmon nanoantennas," *Physical Review Letters,* 101(11), (2008).
[2] S. Wedge, J. A. E. Wasey, W. L. Barnes *et al.*, "Coupled surface plasmon-polariton mediated photoluminescence from a top-emitting organic light-emitting structure," *Applied Physics Letters,* 85(2), 182-184 (2004).
[3] R. L. Olmon, P. M. Krenz, A. C. Jones *et al.*, "Near-field imaging of optical antenna modes in the mid-infrared," *Opt. Express,* 16(25), 20295-20305 (2008).
[4] Q. Song, S. Campione, O. Boyraz *et al.*, "Silicon-based optical leaky wave antenna with narrow beam radiation," *Opt. Express,* 19(9), 8735-8749 (2011).
[5] T. Thio, H. J. Lezec, T. W. Ebbesen *et al.*, "Giant optical transmission of sub-wavelength apertures: physics and applications," *Nanotechnology,* 13(3), 429-432 (2002).
[6] R. Soref, "The Past, Present, and Future of Silicon Photonics," *IEEE J. Sel. Topics. Quantum Electron.,* 12(6), 1678-1687 (2006).
[7] Q. F. Xu, B. Schmidt, S. Pradhan *et al.*, "Micrometre-scale silicon electro-optic modulator," *Nature,* 435(7040), 325-327 (2005).
[8] L. Friedman, R. A. Soref, and J. P. Lorenzo, "Silicon double-injection electro-optic modulator with junction gate control," *J. Appl. Phys.,* 63(6), 1831-1839 (1988).
[9] C. K. Tang, and G. T. Reed, "Highly efficient optical-phase modulator in SOI waveguides," *Electronics Letters,* 31(6), 451-452 (1995).
[10] K. Van Acoleyen, W. Bogaerts, J. Jagerska *et al.*, "Off-chip beam steering with a one-dimensional optical phased array on silicon-on-insulator," *Optics Letters,* 34(9), 1477-1479 (2009).
[11] S. M. Csutak, S. Dakshina-Murthy, and J. C. Campbell, "CMOS-compatible planar silicon waveguide-grating-coupler photodetectors fabricated on silicon-on-insulator (SOI) substrates," *Ieee Journal of Quantum Electronics,* 38(5), 477-480 (2002).
[12] A. A. Oliner, and D. R. Jackson, "Leaky-Wave Antennas," in *Antenna Engineering Handbook*, J. Volakis, Ed., pp. 11.1 - 11.56, McGraw Hill, (2007).

[13] F. Capolino, D. R. Jackson, and D. R. Wilton, "Field representation in periodic artificial materials excited by a source," in *Theory and Phenomena of Metamaterials*, F. Capolino, Ed., pp. 12.1, CRC Press, Boca Raton, FL (2009).
[14] S. Campione, and F. Capolino, "Linear and Planar Periodic Arrays of Metallic Nanospheres: Fabrication, Optical Properties and Applications," in *Selected Topics in Metamaterials and Photonic Crystals*, A. Andreone, A. Cusano, A. Cutolo *et al.*, Ed., pp. World Scientific Publishing, Hackensack, NJ (June 2011).
[15] R. E. Collin, [Antennas and Radiowave Propagation] McGraw Hill, New York(1985).
[16] C. A. Balanis, [Antenna Theory: Analysis and Design] Wiley, (2005).
[17] D. R. Jackson, J. Chen, R. Qiang *et al.*, "The role of leaky plasmon waves in the directive beaming of light through a subwavelength aperture," *Optics Express,* 16(26), 21271-21281 (2008).
[18] R. D. Kekatpure, and M. L. Brongersma, "Near-infrared free-carrier absorption in silicon nanocrystals," *Opt. Lett.,* 34(21), 3397-3399 (2009).
[19] A. W. Elshaari, and S. F. Preble, "10 Gb/s broadband silicon electro-optic absorption modulator," *Optics Communications,* 283(14), 2829-2834 (2010).
[20] S. M. Sze, and K. K. Ng, *Physics of Semiconductor Devices*, Wiley, New York (2007).
[21] M. J. Kerr, and A. Cuevas, "General parameterization of Auger recombination in crystalline silicon," *J. Appl. Phys.,* 91(4), 2473-2480 (2002).
[22] O. Boyraz, X. Sang, E.-K. Tien *et al.*, "Silicon based optical pulse shaping and characterization." 7212, 72120U-13.
[23] W. P. Dumke, "Minority-carrier injection and storage into a heavily doped emitter - Approximate solution for Auger recombination," *Solid-State Electron.,* 24(2), 155-157 (1981).
[24] C. Manolatou, and M. Lipson, "All-Optical Silicon Modulators Based on Carrier Injection by Two-Photon Absorption," *J. Lightwave Technol.,* 24(3), 1433 (2006).